Synthesis and Characterization of Fluorescently Doped Mesoporous Nanoparticles for Two-Photon Excitation

Valérie Lebret,[†] Laurence Raehm,[†] Jean-Olivier Durand,*[,†] Monique Smaïhi,[‡] Corine Gérardin,[†] Nicolas Nerambourg,[§] Martinus H. V. Werts,[§] and Mireille Blanchard-Desce*[,§]

Université Montpellier 2, ENSCM, Institut Charles Gerhardt Montpellier, CNRS, UMR 5253, CC1701 Place Eugène Bataillon, 34095 Montpellier Cedex 05, France, Université Montpellier 2, Institut Européen des Membranes, CNRS, UMR 5635, 1919 Route de Mende, 34293 Montpellier Cedex 05, France, and Université Rennes 1, Institut de Chimie, CNRS, UMR 6510, Campus de Beaulieu, 35042 Rennes Cedex, France

Received December 7, 2007

The template-directed synthesis of mesoporous silica nanoparticles doped with water-soluble fluorescent dyes optimized for two-photon excitation is described. Two structurally related symmetrical two-photon dyes that possess pyridinium acceptor endgroups conjugated to a fluorenyl core are synthesized by Heck coupling. These dyes display bright fluorescence ($\Phi \approx 0.35$) under both one- ($\epsilon \approx 6 \times 10^4$ M^{-1} cm^{-1}) and two-photon excitation ($\sigma_2 \approx 1000$ GM) and were successfully encapsulated in silica nanoparticles via immobilization through noncovalent interactions. The nanoparticles present a mean diameter of 100 nm and a hexagonal network of mesopores as shown by TEM. Interestingly, the photophysical characteristics of the dyes are retained upon their immobilization into the silica matrix, leading to fluorescent silica nanoparticles with giant/unprecedented TPA cross-section (1×10^7 GM). Such nanospheres represent attractive nanoplatforms for the development of biotargeted biocompatible luminescent tracers.

Introduction

Fluorescence labeling of biological materials using small organic dyes is widely used in life sciences, such as in diagnostics and in biological imaging.[1] However, labeling of biomolecules using small organic fluorophores presents certain limitations including photobleaching and low fluorescence signal intensities. These problems might be avoided by the use of nanomaterials, such as luminescent semiconductor quantum dots,[2] fluorescent polystyrene spheres[2,3] or dye-doped silica nanoparticles. The development of dye-doped silica nanoparticles has opened a promising field aiming toward the development of novel luminescent biolabels. Silica nanoparticles are chemically inert and not subject to microbial attacks. Furthermore, the silica matrix porosity is not susceptible to swell or change with a changing pH. In addition, increased photostability may be achieved based on the immobilization of the fluorophores. Therefore, the synthesis and the use of silica nanoparticles for biological devices such as biosensors,[4,5] DNA recognition,[6,7] or cells imaging[8,9] have drawn a lot of scientific attention in the past decade.

Dye-doped silica nanoparticles were first prepared by using the Stöber method via coupling of fluoresceine isothiocyanate dye molecules to (3-aminopropyl)trimethoxysilane.[10] This synthesis is based on ammonia-catalyzed hydrolysis–condensation reactions of tetraethylorthosilicate (TEOS) with water in low molecular weight alcohols and produces uniform silica colloids (100–1000 nm in diameter).[11–13] However, by a modification of the Stöber procedure, using a fluorophore rich core protected within a siliceous shell, Wiesner[14] synthesized smaller nanoparticles in the range of 15 nm. Alternatively, the range of particle sizes is typically reduced from that obtained with the classical Stöber process by synthesizing colloids in microemulsion media.[15–17] A mi-

* Corresponding author. E-mail: durand@univ-montp2.fr (J.-O.D.); mireille.blanchard-desce@univ-rennes1.fr (M.B.-D.). Tel: 33 (0)4 67 14 45 01 (J.-O.D.); 33 (0)2 23 23 62 77 (M.B.-D.; this is fax number as well). Fax: 33 (0)4 67 14 38 52 (J.-O.D.).

[†] Institut Charles Gerhardt Montpellier, Université Montpellier 2.

[‡] Institut Européen des Membranes, Université Montpellier 2.

[§] Institut de Chimie, Université Rennes 1.

(1) Schrock, E.; du Manoir, S.; Veldman, T.; Schoell, B.; Wienberg, J.; Ferguson-Smith, M. A.; Ning, Y.; Ledbetter, D. H.; Bar-Am, I.; Soenksen, D.; Garini, Y.; Ried, T. *Science* **1996**, *273*, 494–497.

(2) Seydack, M. *Biosens. Bioelectron.* **2005**, *20*, 2454–2469.

(3) Ji, J.; Rosenzweig, N.; Griffin, C.; Rosenzweig, Z. *Anal. Chem.* **2000**, *72*, 3497–3503.

(4) Niemeyer, C. M. *Angew. Chem., Int. Ed.* **2001**, *40*, 4128–4158.

(5) Rosi, N. L.; Mirkin, C. A. *Chem. Rev.* **2005**, *105*, 1547–1562.

(6) Zhu, N.; Cai, H.; He, P.; Fang, Y. *Anal. Chim. Acta* **2003**, *481*, 181–189.

(7) Taton, A.; Mirkin, C. A.; Letsinger, R. L. *Science* **2000**, *289*, 1757–1760.

(8) Santra, S.; Zhang, P.; Wang, K.; Tapec, R.; Tan, W. *Anal. Chem.* **2001**, *73*, 4988–4993.

(9) Lin, Y.-S.; Tsai, C.-P.; Huang, H.-Y.; Kuo, C.-T.; Hung, Y.; Huang, D.-M.; Chen, Y.-C.; Mou, C.-Y. *Chem. Mater.* **2005**, *17*, 4570–4573.

(10) Van Blaaderen, A.; Vrij, A. *Langmuir* **1992**, *8*, 2921–31.

(11) Montalti, M.; Prodi, L.; Zaccheroni, N.; Zattoni, A.; Reschiglian, P.; Falini, G. *Langmuir* **2004**, *20*, 2989–2991.

(12) Rossi, L. M.; Shi, L.; Quina, F. H.; Rosenzweig, Z. *Langmuir* **2005**, *21*, 4277–4280.

(13) Wang, L.; Tan, W. *Nano Lett.* **2006**, *6*, 84–88.

(14) Ow, H.; Larson, D. R.; Srivastava, M.; Baird, B. A.; Webb, W. W.; Wiesner, U. *Nano Lett.* **2005**, *5*, 113–117.

(15) Chabra, V.; Pillai, V.; Mishra, B. K.; Morrone, A.; Shah, D. O. *Langmuir* **1995**, *11*, 3307–11.

(16) Arriagada, F. J.; Osseo-Asare, K. *J. Colloid Interface Sci.* **1999**, *211*, 210–220.

10.1021/cm703487b CCC: $40.75
Published on Web 03/04/2008

cromemulsion may be defined as a transparent, isotropic, and thermodynamically stable solution of two immiscible liquids (e.g., water and oil) consisting of microdomains of one liquid stabilized by an interfacial film of surfactant.[18] In water-in-oil microemulsions (reverse microemulsions), the aqueous phase is dispersed as microdroplets (typically 10–25 nm in size) surrounded by a monolayer of surfactant molecules in the continuous hydrocarbon phase. The aqueous cores of microemulsion systems can serve as compartmentalized media for chemical reactions, such as, for example, microreactors for nanoparticle synthesis.[19,20] Recently, several dye-doped silica nanoparticles have been prepared by using the microemulsion water pools as microreactors for the Stöber synthesis.[6,8,9,21–28]

Two types of dyes have commonly been introduced in the silica colloids: rhodamine based chromophores[19,22,26,29] and tris(2,2′-bipyridyl)dichlororuthenium(II).[22,24,25] In order to avoid leakage of chromophores from the particles, studies report the linking of the dye to a silicon alkoxide precursor[22,29] or to a hydrophilic dextran molecule.[19,26] In the case of cationic organometallic species,[6,8,25] encapsulation by a silica matrix inhibits leaching of the compound. In an attempt to prepare biomarkers, the nanoparticles surface may be modified to obtain surface-accessible amine or carboxy groups for further biomolecule conjugation.[21,25,26,29]

Alternatively, a direct microemulsion synthesis method (oil-in-water) provides access to mesoporous nanoparticles. In this case, the organic phase is dispersed as microdroplets surrounded by a monolayer of surfactant molecules in the aqueous medium. In order to prepare mesoporous nanoparticles for further investigation of their properties, we will thus focus on this procedure. Only few studies concerning dye-doped mesoporous nanoparticles have been reported [9,30,31] and, as far as we know, no study dealing with two-photon dye-doped mesoporous MCM-41 nanoparticles has been reported yet. Furthermore, in previously reported studies, the organic chromophores were tethered to the silica matrix through covalent bonds to avoid chromophore leakage from the matrix whereas we decided to use simple electrostatic attraction and steric inclusion for the same purpose.

Recently, two-photon absorption (TPA) by organic chromophores has attracted considerable interest for a wide range of applications such as 3D microfabrication,[32–34] optical data storage,[35] photodynamic therapy,[36,37] optical power limiting,[38–40] and two-photon laser scanning microscopy.[41–43] Indeed, TPA has many attractive features. In particular, it offers the possibility of optically addressing a femtoliter volume element (voxel) within a material that displays TPA due to the high confinement of excitation enabled by selective two-photon excitation. Among the various technical applications of TPA, two-photon fluorescence laser scanning microscopy has gained widespread popularity in the biology community due to the many advantages it provides in biological imaging. This includes, in addition to intrinsic three-dimensional resolution, the possibility to image at increased penetration depth in tissue by replacing typical one-photon excitation in the UV–visible blue region by two-photon excitation in the visible red−NIR region thus resulting in lower scattering losses.

Only a few nanoparticles have been reported for application in two-photon microscopy. Recently, quantum dots encapsulated in amphiphilic polymers were used for multiphoton fluorescence imaging of mice tissues in vivo.[44] Folic acid conjugated quantum dots were delivered into folate-receptor positive cell lines (KB human epithelial oral carcinoma cells) and two-photon imaging of these cells was described.[45] Prasad et al. also described ZnS[46] and Fe_2O_3[47] core nanoparticles in a silica shell, with a covalently attached two-photon dye. These nanoparticles were successfully used for imaging KB cells. Very recently, the same group reported two-photon imaging and photodynamic therapy of HeLa cells

(17) Lopez-Quintela, M. A. *Curr. Opin. Colloid Interface Sci.* **2003**, *8*, 137–144.
(18) De Gennes, P. G.; Taupin, C. *J. Phys. Chem.* **1982**, *86*, 2294–304.
(19) Arriagada, F. J.; Osseo-Assare, K. *J. Colloid Interface Sci.* **1995**, *170*, 8–17.
(20) Lopez-Quintela, M. A.; Tojo, C.; Blanco, M. C.; Garcia Rio, L.; Leis, J. R. *Curr. Opin. Colloid Interface Sci.* **2004**, *9*, 264–278.
(21) Santra, S.; Yang, H.; Dutta, D.; Stanley, J. T.; Holloway, P. H.; Tan, W.; Moudgil, B. M.; Mericle, R. A. *Chem. Commun.* **2004**, 2810–2811.
(22) Lian, W.; Litherland, S. A.; Badrane, H.; Tan, W.; Wu, D.; Baker, H. V.; Gulig, P. A.; Lim, D. V.; Jin, S. *Anal. Biochem.* **2004**, *334*, 135–144.
(23) Zhao, X.; Hilliard, L. R.; Wang, K.; Tan, W. In *Encyclopedia of Nanoscience and Nanotechnology*; Nalwa, H. S., Ed.; American Scientific Publishers: Valenica, CA, 2004; Vol. 1, pp 255−268.
(24) Zhao, X.; Bagwe, R. P.; Tan, W. *Adv. Mater.* **2004**, *16*, 173–176.
(25) Bagwe, R. P.; Yang, C.; Hilliard, L. R.; Tan, W. *Langmuir* **2004**, *20*, 8336–8342.
(26) Yang, W.; Zhang, C. G.; Qu, H. Y.; Yang, H. H.; Xu, J. G. *Anal. Chim. Acta* **2004**, *503*, 163–169.
(27) Jain, T. K.; Roy, I.; De, T. K.; Maitra, A. *J. Am. Chem. Soc.* **1998**, *120*, 11092–11095.
(28) Wang, L.; Yang, C.; Tan, W. *Nano Lett.* **2005**, *5*, 37–43.
(29) Yang, H.-H.; Qu, H.-Y.; Lin, P.; Li, S.-H.; Ding, M.-T.; Xu, J.-G. *Analyst* **2003**, *128*, 462–466.
(30) Fowler, C. E.; Khushalani, D.; Lebeau, B.; Mann, S. *Adv. Mater.* **2001**, *13*, 649–652.
(31) Slowing, I.; Trewyn, B. G.; Lin, V. S.-Y. *J. Am. Chem. Soc.* **2006**, *128*, 14792–14793.
(32) Kawata, S.; Sun, H.-B.; Tanaka, T.; Takada, K. *Nature* **2001**, *412*, 697.
(33) Zhou, W.; Kuebler, S. M.; Braun, K. L.; Yu, T.; Cammack, J. K.; Ober, C. K.; Perry, J. W.; Marder, S. R. *Science* **2002**, *296*, 1106–1109.
(34) Cumpston, B. H.; Ananthavel, S. P.; Barlow, S.; Dyer, D. L.; Ehrlich, J. E.; Erskine, L. L.; Heikal, A. A.; Kuebler, S. M.; Lee, I. Y. S.; McCord-Maughon, D.; Qin, J.; Rockel, H.; Rumi, M.; Wu, X.-L.; Marder, S. R.; Perry, J. W. *Nature* **1999**, *398*, 51–54.
(35) Parthenopoulos, D. A.; Rentzepis, P. M. *Science* **1989**, *245*, 843–5.
(36) Gao, D.; Agayan, R. R.; Xu, H.; Philbert, M. A.; Kopelman, R. *Nano Lett.* **2006**, *6*, 2383–2386.
(37) Kim, S.; Ohulchanskyy, T. Y.; Pudavar, H. E.; Pandey, R. K.; Prasad, P. N. *J. Am. Chem. Soc.* **2007**, *129*, 2669–2675.
(38) He, G. S.; Bhawalkar, J. D.; Zhao, C. F.; Prasad, P. N. *Appl. Phys. Lett.* **1995**, *67*, 2433–2435.
(39) Ehrlich, J. E.; Wu, X. L.; Lee, I. Y. S.; Hu, Z. Y.; Rockel, H.; Marder, S. R.; Perry, J. W. *Opt. Lett.* **1997**, *22*, 1843–1845.
(40) Charlot, M.; Izard, N.; Mongin, O.; Riehl, D.; Blanchard-Desce, M. *Chem. Phys. Lett.* **2006**, *417*, 297–302.
(41) Denk, W.; Strickler, J. H.; Webb, W. W. *Science* **1990**, *248*, 73–6.
(42) Xu, C.; Zipfel, W.; Shear, J. B.; Williams, R. M.; Webb, W. W. *Proc. Natl. Acad. Sci. U.S.A.* **1996**, *93*, 10763–8.
(43) Zipfel, W. R.; Williams, R. M.; Christie, R.; Nikitin, A. Y.; Hyman, B. T.; Webb, W. W. *Proc. Natl. Acad. Sci. U.S.A.* **2003**, *100*, 7075–7080.
(44) Larson, D. R.; Zipfel, W. R.; Williams, R. M.; Clark, S. W.; Bruchez, M. P.; Wise, F. W.; Webb, W. W. *Science* **2003**, 1434–1436.
(45) Bharali, D. J.; Lucey, D. W.; Jayakumar, H.; Pudavar, H. E.; Prasad, P. N. *J. Am. Chem. Soc.* **2005**, *127*, 11364–11371.
(46) Lal, M.; Levy, L.; Kim, K. S.; He, G. S.; Wang, X.; Min, Y. H.; Pakatchi, S.; Prasad, P. N. *Chem. Mater.* **2000**, *12*, 2632–2639.
(47) Levy, L.; Yudhisthira Sahoo; Kim, K.-S.; Bergey, E. J.; Prasad, P. N. *Chem. Mater.* **2002**, *14*, 3715–3721.

Scheme 1. Synthesis of Chromophores (a) 2 and (b) 5

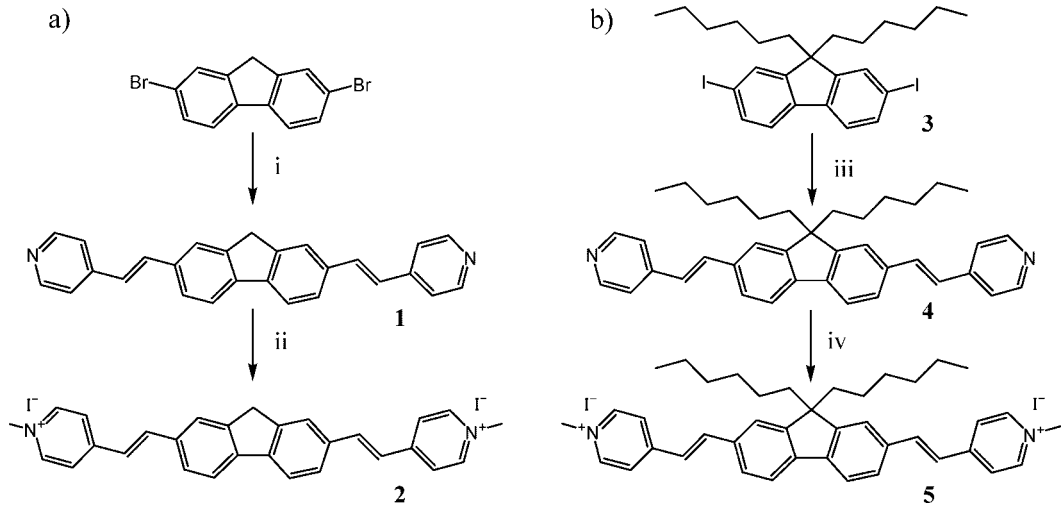

(i) 4-Vinylpyridine, $Pd(OAc)_2$, triorthotolylphosphine (TOP), Et_3N, DMF, CH_3CN, 85%; (ii) CH_3I, MeCN, 77%; (iii) 4-vinylpyridine, $Pd(OAc)_2$, triorthotolylphosphine, Et_3N, DMF, AcOEt, 46%; (iv) CH_3I, MeCN, 95%.

by using two-photon fluorescent dye nanoaggregates[37] which transfer excitation energy to a photosensitizing PDT drug. Both the dye and the PDT drug were encapsulated in a hybrid silica nanoparticle. Mancin[48] prepared organosilica nanoparticles doped with two-photon absorbing distyrylbenzene derivatives. Those nanoparticles were used for two-photon imaging of esophageal carcinoma KYSE-510 cells. Finally, very recently, fully organic nanoparticules ("nanodots") of a few nanometers size with unprecedented one- and two-photon absorption cross-sections[49,50] have been reported. This provided evidence that the gathering of a large number (up to almost 100 in the latter case) of optimized two-photon fluorophores within single nanoparticles can effectively lead to brilliant nano-objects with giant TPA cross-sections. Following this route, our strategy has been to confine an even larger number of two-photon fluorophores within single nanobjects by encapsulating them in mesopourous silica nanoparticles. This requires the use of suitable fluorophores being both water-soluble and showing large two-photon absorption cross sections (σ_2) in the spectral range of interest for biological imaging (700–1200 nm) while maintaining sizable fluorescence quantum yield (Φ) in water. With this aim in mind, we have prepared quadrupolar water-soluble derivatives bearing pyridinum end-groups grafted on a fluorenyl core moiety. Quadrupolar derivatives, i.e. symmetrical conjugated molecules bearing two electron-releasing (D) or electron-withdrawing (A) end-groups, can indeed display very high TPA cross sections, larger than their dipolar (push–pull) counterpart,[51] in relation with a quadrupolar intramolecular charge transfer taking place between the ends and the center of the molecules.[52] Earlier work has shown that both push-push (bis-donor) and pull-pull (bis-acceptor) derivatives built from a biphenyl core show significant TPA in the target spectral range of interest[53,54] and increasing the strength of donor or acceptor end-groups results in increased TPA response. In addition, elongated amphiphilic derivatives could be used for nondamaging membrane and cell imaging.[55,56] We turned to bis-pyridinium derivatives (compounds **2** and **5** in Scheme 1) because this acceptor moiety is both liable to provide water solubility, as well as large σ_2 when grafted onto cores such as diacetylene π-bridges, phenylene,[57] pyrrole,[58] dihydrophenanthrene,[55,59] or fluorene.[60] The TPA properties in water of such derivatives have not been studied previously and are reported in this paper. In the following, we first describe the synthesis of these water-soluble organic chromophores and investigate their TPA properties in solution. We then report their incorporation in mesoporous silica nanoparticles without covalent linkage via a direct microemulsion synthesis process. Finally the photophysical and TPA properties of the resulting two-photon dyes doped silica nanoparticles are presented, providing evidence that the implemented route actually lead to fluorescent silica nanoparticles with giant TPA cross-sections

(48) Bertazza, L.; Celotti, L.; Fabbrini, G.; Loi, M. A.; Maggini, M.; Mancin, F.; Marcuz, S.; Menna, E.; Muccini, M.; Tonellato, U. *Tetrahedron* **2006**, *62*, 10434–10440.
(49) Mongin, O.; Krishna, T. R.; Werts, M. H. V.; Caminade, A.-M.; Majoral, J.-P.; Blanchard-Desce, M. *Chem. Commun.* **2006**, 915–917.
(50) Mongin, O.; Pla-Quintana, A.; Terenziani, F.; Drouin, D.; Le Droumaguet, C.; Caminade, A.-M.; Majoral, J.-P.; Blanchard-Desce, M. *New J. Chem.* **2007**, *31*, 1354–1367.
(51) Barzoukas, M.; Blanchard-Desce, M. *J. Chem. Phys.* **2000**, *113*, 3951–3959.
(52) Rumi, M.; Ehrlich, J. E.; Heikal, A. A.; Perry, J. W.; Barlow, S.; Hu, Z.; McCord-Maughon, D.; Parker, T. C.; Röckel, H.; Thayumanavan, S.; Marder, S. R.; David Beljonne; Brédas, J.-L. *J. Am. Chem. Soc.* **2000**, *122*, 9500–9510.
(53) Mongin, O.; Porres, L.; Moreaux, L.; Mertz, J.; Blanchard-Desce, M. *Org. Lett.* **2002**, *4*, 719–722.
(54) Mongin, O.; Porres, L.; Chariot, M.; Katan, C.; Blanchard-Desce, M. *Chem.—Eur. J.* **2007**, *13*, 1481–1498.
(55) Blanchard-Desce, M. *C. R. Phys.* **2002**, *3*, 439–448.
(56) Ventelon, L.; Charier, S.; Moreaux, L.; Mertz, J.; Blanchard-Desce, M. *Angew. Chem., Int. Ed.* **2001**, *40*, 2098–2101.
(57) Iwase, Y.; Kamada, K.; Ohta, K.; Kondo, K. *J. Mater. Chem.* **2003**, *13*, 1575–1581.
(58) Abbotto, A.; Beverina, L.; Bozio, R.; Facchetti, A.; Ferrante, C.; Pagani, G. A.; Pedron, D.; Signorini, R. *Org. Lett.* **2002**, *4*, 1495–1498.
(59) Blanchard-Desce, M. H.; Ventelon, L.; Charier, S.; Moreaux, L.; Mertz, J. *Proc. SPIE—Int. Soc. Opt. Eng.* **2001**, *4461*, 20–32.
(60) Kawamata, J.; Akiba, M.; Tani, T.; Harada, A.; Inagaki, Y. *Chem. Lett.* **2004**, *33*, 448–449.

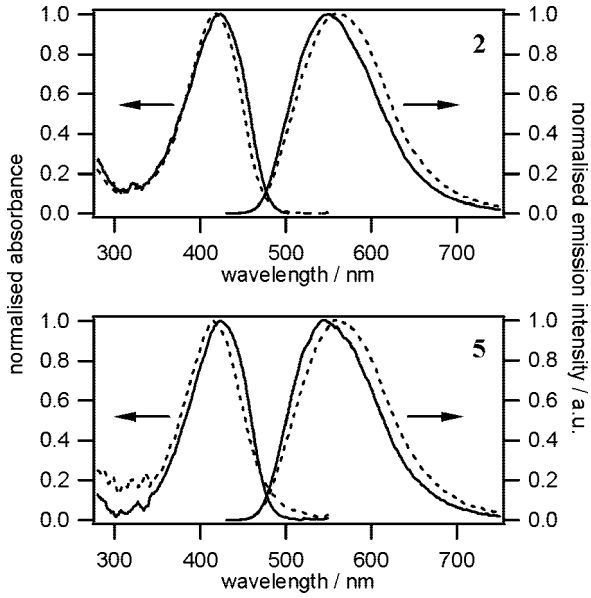

Figure 1. Normalized UV/vis absorption and fluorescence emission spectra of dilute solutions (1.5 μM) of **2** and **5** in ethanol (solid lines) and water (dashed). The fluorescence was excited at the wavelength of maximum absorbance.

(1×10^7 GM) of interest for sensitive detection by two-photon excited fluorescence.

Results and Discussion

Synthesis and Photophysical Properties of the Two-Photon Fluorescent Dyes. Compounds **2** and **5** were synthesized as described in Scheme 1, starting from dihalogenated fluorene cores that were extended through Heck coupling with vinylpyridine.

Compound **1** was synthesized following the literature procedure[45] by reacting dibromofluorene with 4-vinylpyridine and by using $Pd(OAc)_2$ TOP as catalyst instead of $Pd(PPh_3)_4$. Methylation[61] of derivative **1** gave chromophore **2**. Diiodo derivative **3** was synthesized according to the literature.[53,62] The Heck reaction of compound **3** with 4-vinylpyridine afforded compound **4**. Methylation of compound **4** gave chromophore **5**.

Compounds **2** and **5** are soluble and fluorescent in ethanol and water, although the solubility of **5** in these solvents is reduced ($<1 \times 10^{-4}$ M) compared to **2** ($>1 \times 10^{-3}$ M) by the introduction of the apolar, lipophilic *n*-hexyl chains. Steady-state optical absorption and emission spectra of both chromophores in solution are shown in Figure 1. The spectra of **2** and **5** are similar, indicating that the introduction of the hexyl chains does not essentially alter the basic photophysical features of the chromophore. The absorption band of both **2** and **5** undergoes a small hypsochromic shift upon going from ethanol to water, whereas the fluorescence emission displays a small bathochromic shift, leading to a slightly larger Stokes' shift in ethanol compared to water. Such solvent polarity shifts are similar to what was reported for cationic push–pull chromophores with pyridinium acceptor moieties, in relation with combined larger stabilization of the ground-state with respect to the excited-state (as a result of higher charges localization in the ground state) and increase of the reorganization energy with increased solvent polarity.[63]

Table 1. Optical Spectroscopic Data for Chromophores 2 and 5 Free in Solution

		absorption		emission	
compd	solvent	λ_{max} (nm)	ϵ (M^{-1} cm^{-1})	λ_{max} (nm)	Φ
2	EtOH	425	6.2×10^4	551	0.33
2	H_2O	414	5.9×10^4	562	0.35
5	EtOH	423	[a]	541	0.38
5	H_2O	418	[a]	556	0.27

[a] Extinction coefficient not determined because of limited solubility.

Table 2. Steady-State Anisotropies (r, measured under excitation into the longest-wavelength absorption band) and Fluorescence Decay Times (τ) for Chromophores 2 and 5 Free in Solution ($T = 298$ K)

	solvent	r	τ (ns)
2	EtOH	0.136	1.03
2	H_2O	0.110	1.11
5	EtOH	0.136	1.14
5	H_2O	0.107	1.18

Quantitative data from the steady-state absorption and emission measurements are listed in Table 1. The molar extinction coefficient of **2** shows the sizable values typical of this family of quadrupolar fluorene-based chromophores.[54] The extinction coefficient of **5** could not be determined reliably as a result of its limited solubility, but is not expected to differ significantly from that of **2**, in view of the similarity of the shapes of the absorption and emission spectra shown in Figure 1. Interestingly, both **2** and **5** retain reasonable fluorescence quantum yields in water. This indicates that - contrarily to cationic quadrupolar water-soluble derivatives built from the same core but bearing neutral electron-donating engroups, which shows major reduction of both their fluorescence quantum yield (quenching) and TPA cross-section,[64] the functionalization with pyridinium end-groups does not favor deleterious aggregation processes.

The fluorescence lifetimes of **2** and **5** have been measured, and were all found to be around 1.1 ns (Table 2). The rotational dynamics of both chromophores in solution were probed using steady-state fluorescence anisotropy measurements. The steady-state anisotropy of the fluorescence emission yields information on how much the molecules rotate during their excited-state lifetime,[65] and is influenced by the size of the fluorescent object and the viscosity of the surrounding medium. The increased anisotropy in ethanol is due to the higher viscosity of this solvent compared to water. The observed anisotropy values are in line with fluorescent objects of an estimated 0.75 nm hydrodynamic radius (calculated using the Perrin equation, a fluorescence lifetime of 1.1 ns and assuming a limiting anisotropy r_0 of 0.35).[65]

(61) Blanchard-Desce, M.; Arrhenius, T. S.; Lehn, J.-M. *Bull. Soc. Chim. Fr.* **1993**, *130*, 266–272.
(62) Cao, X.-Y.; Zi, H.; Zhang, W.; Lu, H.; Pei, J. *J. Org. Chem.* **2005**, *70*, 3645–3653.
(63) Laage, D.; Thompson, W. H.; Blanchard-Desce, M.; Hynes, J. T. *J. Phys. Chem. A* **2003**, *107*, 6032–6046.
(64) Thatavarathy, R. K.; Parent, M.; Werts, M. H. V.; Moreaux, L.; Gmouh, S.; Charpak, S.; Caminade, A.-M.; Majoral, J.-P.; Blanchard-Desce, M. *Angew. Chem., Int. Ed.* **2006**, *45*, 4645–4648.
(65) Valeur, B. *Molecular Fluorescence: Principles and Applications*; Wiley-VCH: Weinheim, Germany, 2002.

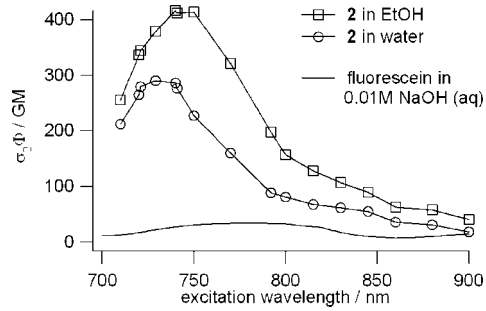

Figure 2. Two-photon excitation spectrum of the fluorescence of free **2** in solution (1×10^{-4} M). The two-photon excitation spectrum of fluorescein has been added for comparison. The spectrum is expressed as the two-photon excitation action cross sections, the product of the fluorescence quantum yield Φ and the two-photon absorption cross section σ_2 (1 GM = 1×10^{-50} cm^4 s photon).

The fluorescence response of **2** toward two-photon excitation was evaluated quantitatively using two-photon excited fluorescence (TPEF) spectroscopy (Figure 2). Quantitative TPEF measurements were not possible for compound **5** due to the aforementioned solubility problems. In view of the structural similarity between **2** and **5** no significant differences in two-photon response are expected. The chromophore exhibits a strong response toward two-photon excitation between 700 and 900 nm, its two-photon excited fluorescence being approximately ten times as efficient as that of benchmark fluorophore fluorescein. The TPEF excitation spectrum displays a maximum near 740 nm, which is a shorter wavelength than twice the wavelength of the one-photon absorption maximum. The intense two-photon absorption band originates from a transition into a higher excited-state that is forbidden under one-photon excitation, but strongly allowed under two-photon conditions.[51,52,66] As a result, the (weaker) two-photon absorption band corresponding to excitation into the first electronic transition only appears as a shoulder in the TPEF excitation spectrum, indeed at twice the wavelength of the one-photon absorption maximum (approximately 840 nm) due to slight deviation from ideal symmetry as already reported for similar bis-donor quadrupolar chromophores.[67]

The combination of a reasonable fluorescence quantum yield with high one-photon and very high two-photon absorption cross-sections makes water-soluble chromophore **2**, and its more hydrophobic derivative **5**, interesting candidates for inclusion into silica nanoparticles.

Synthesis and Photophysical Properties of Dye-Doped Silica Nanoparticles. The synthesis of the nanoparticles was performed using template-directed synthesis following a procedure similar to that used by Mann et al.[30] We obtained particles presenting an homogeneous size by controlled quenching of an alkaline reaction mixture containing cetyltrimethylammonium bromide (CTAB), chromophore **2** or **5** and tetraethoxysilane (TEOS). The temperature and stirring time of the mixture were found to be crucial parameters to control both formation and size of the nanoparticles. Longer stirring times lead to bigger objects. Past a critical time (around 8 min), the particles began to precipitate and the aggregates cannot be reversed to colloidal solution again. The temperature is controlled (25 °C) during the whole synthesis process. Nanoparticles **NP-2** (which encapsulate chromophore **2**) or nanoparticles **NP-5** (which encapsulate chromophore **5**) were centrifuged three times, then washed with EtOH in a Soxhlet for 24 h. The surfactant removal was monitored by IR spectroscopy.

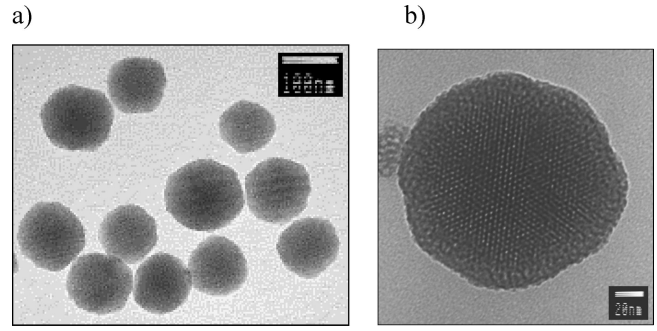

Figure 3. (a) TEM image of the nanoparticles (scale bar = 100 nm). (b) High-resolution image of a single nanoparticle showing the hexagonal networks of mesopores (scale bar = 20 nm).

Table 3. Data from Dynamic Light Scattering on Suspensions of Nanoparticles[a]

sample	PDI	D_h (nm)
NP-2	0.06	127
NP-5	0.04	150

[a] PDI, polydispersity index from the method of cumulants; D_h, hydrodynamic diameter.

Table 4. BET Analysis Data

sample	S_{BET}[a] (m^2 g^{-1})	total pore volume[b]	average pore size (nm)
NP-2	727	0.45	1.7
NP-5	644	0.66	1.8

[a] S_{BET}, specific surface area. [b] Calculated from the desorption branch using the BJH method.

Transmission electron microscopy (TEM) of the materials and dynamic light scattering (DLS) showed the presence of a large number of monodisperse nanoparticles (Figure 3a). The average diameter of a nanoparticle was determined to be about 100 nm by TEM. The nanoparticles show a mesoporous structured network (Figure 3b). A good agreement between the TEM and DLS measurements was noticed. The particles appeared spherical with a fairly low polydispersity (Table 3). The hydrodynamic diameters (D_h) for **NP-2** and **NP-5** were determined to be 127 and 150 nm, respectively. These are the intensity-averaged values of the hydrodynamic diameters, which are obtained from the *z*-averaged translational diffusion coefficients calculated by the cumulant method. The cumulant method is valid here since the values of the polydispersity index are considerably low. Because of the intensity weighting of the average hydrodynamic size, the mean D_h values are slightly larger than the average values of sizes determined from TEM. Surface area analysis using the BET (Brunauer–Emmett–Teller) method (Table 4) show that nanoparticles **NP-2** and **NP-5** are mesoporous. Pore size is around 1.8 nm and the surface area is quite large, with a 700 m^2 g^{-1} average value.

(66) Katan, C.; Terenziani, F.; Mongin, O.; Werts, M. H. V.; Porres, L.; Pons, T.; Mertz, J.; Tretiak, S.; Blanchard-Desce, M. *J. Phys. Chem. A* **2005**, *109*, 3024–3037.
(67) Katan, C.; Tretiak, S.; Werts, M. H. V.; Bain, A. J.; Marsh, R. J.; Leonczek, N.; Nicolaou, N.; Badaeva, E.; Mongin, O.; Blanchard-Desce, M. *J. Phys. Chem. B* **2007**, *111*, 9468–9483.

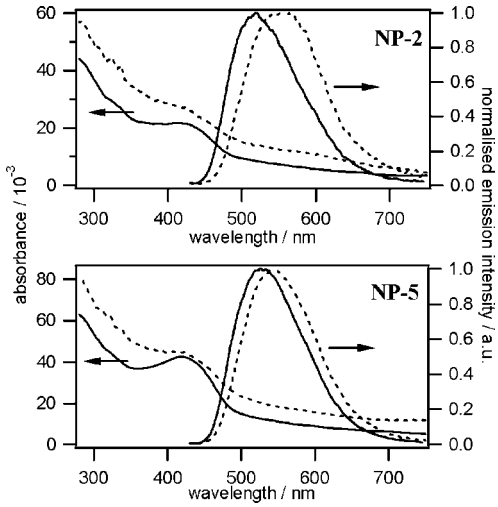

Figure 4. Absorption (left axis) and emission spectra (right axis) of nanoparticles **NP-2** (top) and **NP-5** (bottom) in ethanol (solid line) and water (dashes). The fluorescence was excited at 418 nm.

Subsequently, the particles were characterized by optical absorption and emission spectroscopy. For each type of particles (**NP-2** and **NP-5**) three independently prepared batches were studied to verify reproducibility and to obtain an estimate of the extent of batch-to-batch variations in photophysical properties. Steady-state absorption and emission spectra of dilute suspensions of the particles in water and ethanol (Figure 4) reveal the presence of the encapsulated chromophore inside the particles: the typical dye-related absorption ($\lambda_{max} \approx 420$ nm) and emission bands ($\lambda_{max} \approx 540$ nm) can be distinguished. The extensive Soxhlet extraction applied ensures removal of free dyes, but does not remove the encapsulated chromophores, demonstrating that these are well retained inside the particles. This provides evidence that immobilization of cationic dyes **2** and **5** via Coulombic interactions and steric exclusion is a valid strategy.

The fluorescence emission spectra of the encapsulated chromophores are still sensitive to the solvent, meaning that solvent can penetrate the pores of the particles, but that the relatively rigid rodlike chromophores (whose length is about 2.35 nm) are too large to escape from the particle, which reflects the mesoporous nature of the particles found in the BET analysis.

The solvatochromic shift between ethanol and water is actually more pronounced for the nanoparticles than for the free dyes, which stems from the fact that the emission of the particles in ethanol is significantly blue-shifted compared to the free dye in ethanol, whereas the effect of encapsulation on the emission wavelength is much less pronounced for water. The blue-shifted emission of the encapsulated dyes as compared to the free dyes is indicative of reduced reorganization energy, in relation with the lower accessibility of solvating molecules. This effect is expected to be less pronounced for (smaller) water molecules as compared to ethanol molecules.

The absorption spectra of the particle suspensions show a significant contribution from light scattering by the silica particles. The dye-related absorption band is superimposed onto this baseline. Quantitative determination of dye absorbance was achieved by subtracting the scatter component

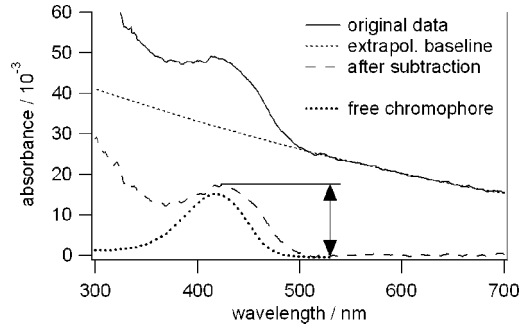

Figure 5. Typical baseline substraction (see text) yielding the dye absorbance (long dashes, **NP-5** in water). The absorption of the free dye has been added for comparison.

Table 5. Dye Doping Levels of NP-2 and NP-5 Silica Nanoparticles, Derived from UV/vis Data

	μmol/g[a]	mmol/L[b]	chromophores per particle [c]
NP-2	1.9 ($\pm$ 0.5)	4.2	4.4×10^3
NP-5	3.8 ($\pm$ 0.7)	8.4	8.9×10^3

[a] Based on UV/vis spectrometry of nanoparticle suspensions. Value between parentheses is the standard deviation between batches. [b] Calculated using a density of silica of 2.2 kg/L.[48] [c] Estimated using a spherical particle diameter of 150 nm.

using the following procedure (exemplified in Figure 5). The region from 520 to 680 nm, which contains no contributions from dye absorption bands, was taken as a model of the baseline. The model baseline was extrapolated using a second-order polynomial. The extrapolated baseline was subtracted from the initial absorption spectrum, revealing clearly the dye-related absorption spectrum. The quadratic baseline extrapolation breaks down for wavelengths shorter than 400 nm, but because the absorption maximum of interest is situated near 420 nm this is not a problem. The procedure was automated and carried out consistently on all relevant spectra of nanoparticle suspensions, always obtaining a clear residual dye absorption band.

The dye content of the particles can be estimated from the UV/vis absorbance data, using the dye absorbance of a suspension of known particle mass concentration and the extinction coefficient of the free dye, which is not expected to change significantly upon inclusion into the silica particles (the shapes and positions of the absorption and emission spectra are similar for free and encapsulated dye). With an estimated density of 2.2 kg/L for mesoporous silica,[48] and a particle diameter of 150 nm, we arrive at estimates of several thousands of dye molecules per particle (Table 5), with chromophore **5** giving a slightly higher doping level than **2**.

The (baseline-subtracted) dye absorbance is also instrumental in determining the fluorescence quantum yields of the nanoparticles, listed in Table 6. The values reported are averages over the three batches. Fluorescence quantum yields were reproducible within $\pm$30% of the reported average. The quantum yields are generally higher than for the free dyes in solution, indicating a beneficial effect of the encapsulation, and the absence of deleterious intraparticle interchromophore interactions. The absence of interchromophore energy transfer is evident from the high values of the fluorescence anisotropy for the particles. Energy migration within the particles would

Table 6. Monophotonic Fluorescence Emission Data for Dye-Doped Silica Nanoparticles NP-2 and NP-5: Wavelength of Emission Maximum (λ_{em}), Fluorescence Quantum Yield (Φ), Steady-State Anisotropy (r), and Average Fluorescence Lifetime[a]

	solvent	λ_{em} (nm) [b]	Φ^b	r^b	$<\tau>$ (ns)[c]
NP-2	EtOH	521	0.43	0.355	1.26
NP-2	H_2O	563	0.28	0.293	1.38
NP-5	EtOH	525	0.52	0.292	1.33
NP-5	H_2O	541	0.43	0.310	1.44

[a] The measured nanoparticle fluorescence quantum yields were found to be reproducible within ±30% between different, independently prepared batches of nanoparticles. [b] Average over three independently prepared batches of particles [c] Nanoparticle fluorescence shows nonmonoexponential decay. Reported are the average lifetimes. See Text.

lead to depolarisation and subsequently to lower anisotropies. Compared to the free dyes, which have anisotropies in the 0.10–0.14 range (Table 2), the emission anisotropy of the particles is close to the theoretical (0.4) and experimentally observed (0.36) limits. This demonstrates that the measured fluorescence does not stem from free chromophores in solution (which would display the anisotropy corresponding to free chromophores) and that the dyes are effectively immobilized inside the 150 nm diameter nanoparticles.

In time-correlated single-photon counting (TCSPC) measurements, the fluorescence of the dye-doped nanoparticles shows a nonmonoexponential decay, indicative of a distribution of different dye encapsulation sites within the particles. In absence of a detailed microscopic model of the dye inclusion (which would require more detailed photophysical and structural studies), the decay curves can generally be adequately described by the sum of two exponentials, a shorter component (~0.5 ns) and a longer component (~1.5 ns), and in Table 6 we report the average fluorescence lifetime, a weighted average of both components, in order to facilitate comparison. The fluorescence lifetimes are slightly longer for the encapsulated dyes compared to the free dyes. In combination the slightly higher fluorescence quantum yields of the dyes, this reveals that nonradiative decay is slowed down for encapsulated dyes. Such feature further confirms the efficient immobilization of the dyes in the silica mesoporous structures.

The preservation (and even slight augmentation) of efficient fluorescence emission from the dyes upon encapsulation is promising for the generation of nanoparticle fluorescence under two-photon excitation. Under excitation with near-infrared femtosecond light pulses, the doped nanoparticles do indeed show two-photon excited fluorescence (TPEF) emission (Figure 6). The TPEF emission spectra are identical to their monophotonic (OPEF) counterparts, and the fluorescence intensity depends quadratically on the excitation power, indicative of pure two-photon excitation without saturation or photobleaching.

The response of the doped particle fluorescence toward two-photon excitation has been quantified by measuring the two-photon excitation action cross sections $\sigma_2\Phi$ as a function of excitation wavelength.[68] These cross sections are the product of the fluorescence quantum yield Φ and the two-photon absorption cross sections σ_2, the latter being expressed

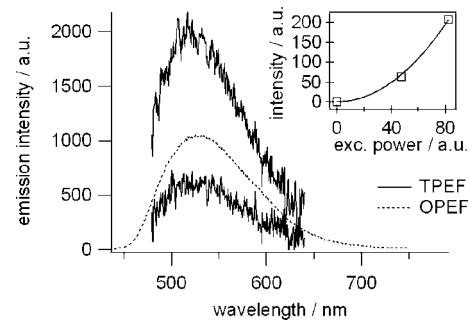

Figure 6. Example of two-photon excited fluorescence (TPEF) of the dye-doped nanoparticles in suspension (**NP-5** in ethanol, excited at 740 nm using a femtosecond modelocked Ti:sapphire laser). The solid lines are the TPEF emission spectra at two different excitation powers, the dotted line is the one-photon excited emission (excited at 418 nm, using a Xe lamp). The inset shows the quadratic dependence of the emission intensity on excitation power.

in Göppert-Mayer units (1 GM equals 1×10^{-50} cm^4 s photons). The excited state from which emission takes place is identical for both one and two-photon excitation (and generally does not depend on the excitation wavelength, following the well-known empirical Kasha−Vavilov rule [69]). Therefore the fluorescence quantum yield is the same under one- and two-photon excitation. The product $\sigma_2\Phi$ is a direct and quantitative measure of the "brightness" of a fluorophore under two-photon excitation, in analogy to the monophotonic brightness $\epsilon\Phi$, the product of the extinction coefficient and the fluorescence quantum yield.

In the measured spectra (Figure 7), the two-photon excitation action cross sections $\sigma_2\Phi$ are expressed on a "per chromophore" basis as this allows for a direct comparison with the free dyes, and an assessment of the effect of encapsulation on the TPEF performance of the dyes. The actual chromophore concentration in the nanoparticle samples was established using UV/vis spectrometry, according to the procedure described above, as this is the most reliable method. Taking into account the experimental uncertainty of dye concentration, a significant change in two-photon excitation cross sections is not observed for encapsulated dyes, compared to free dyes in solution. This means that the good two-photon response of the dyes is retained upon encapsulation.

The combination of the estimates of the numbers of chromophores per particle and the values of $\sigma_2\Phi$ per encapsulated chromophore yield the two-photon excitation action cross sections per particle. For **NP-5** in water this leads for example to a giant value of 3.6×10^6 GM, corresponding to a two-photon absorption cross section σ_2 of about 1×10^7 GM (10 MGM). This giant value is to be put in perspective considering the large size of the nanoparticles

(68) Xu, C.; Webb, W. W. *J. Opt. Soc. Am. B* **1996**, *13*, 481–491.

(69) Braslavsky, S. E.; Acuna, A. U.; Adam, W.; Amat, F.; Armesto, D.; Atvars, T. D. Z.; Bard, A.; Bill, E.; Bjoern, L. O.; Bohne, C.; Bolton, J.; Bonneau, R.; Bouas-Laurent, H.; Braun, A. M.; Dale, R.; Dill, K.; Doepp, D.; Duerr, H.; Fox, M. A.; Gandolfi, T.; Grabowski, Z. R.; Griesbeck, A.; Kutateladze, A.; Litter, M.; Lorimer, J.; Mattay, J.; Michl, J.; Miller, R. J. D.; Moggi, L.; Monti, S.; Nonell, S.; Ogilby, P.; Olbrich, G.; Oliveros, E.; Olivucci, M.; Orellana, G.; Prokorenko, V.; Naqvi, K. R.; Rettig, W.; Rizzi, A.; Rossi, R. A.; San Roman, E.; Scandola, F.; Schneider, S.; Thulstrup, E. W.; Valeur, B.; Verhoeven, J.; Warman, J.; Weiss, R.; Wirz, J.; Zachariasse, K. *Pure Appl. Chem.* **2007**, *79*, 293–465.

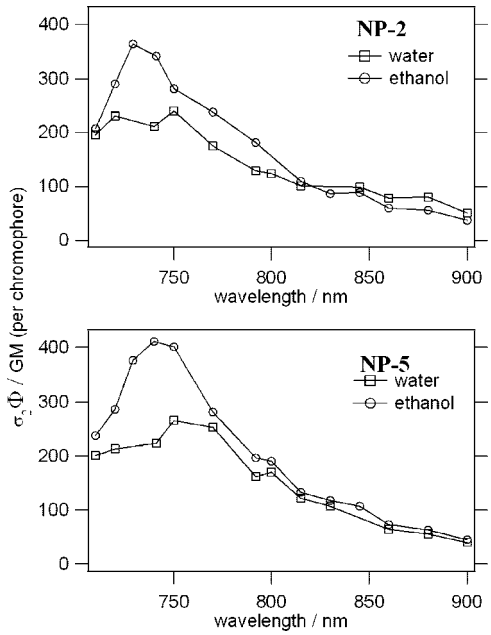

Figure 7. Two-photon excitation profiles for the fluorescence of silica nanoparticles doped with **2** (top) and **5** (bottom) in water and ethanol. The spectra are reported in two-photon excitation cross-sections per chromophore. Because of the relatively large uncertainties in the determination of the exact dye concentration in the samples, the relative error on the absolute values is estimated to be ±20%.

(150 nm diameter) compared to molecules (~1 nm) and luminescent semiconductor quantum dots (~10 nm) or organic nanodots[49] (a few nm). Indeed, because of the very high number of two-photon fluorophores encapsulated within a single nanoparticle (i.e., several thousands), unprecedented TPA cross-section could be obtained, leading to the brightest two-photon fluorescent water-soluble nanoparticles ever reported. For these reasons, these water-soluble fluorescent nano-objects open attractive perspectives for single particle detection. Given the possibility for further surface functionlization (including grafting of recognition and targeting moiety) such nanotools could be of major interest for sensitive detection and diagnostics.

Conclusion

Two structurally closely related fluorescent chomophores were synthesized. The chromophores show appreciable fluorescence in ethanolic and aqueous solution, and respond well to two-photon excitation with near-infrared pulsed laser light. Interestingly, chromophore **2** was found to be very soluble in water while retaining its two-photon brightness, and it is 10 times more efficient than fluorescein at certain excitation wavelengths. Both chromophores were successfully encapsulated in silica nanoparticles possessing a hexagonal network of mesopores. The photophysical study reveals that the immobilization of the chromophores in the silica network is indeed effective even in the absence of covalent interactions. As a result of the immobilization of the fluorescent chromophores, no leaching is observed and the quantum yields are generally higher for the doped nanoparticles than for the free chromophores in solution, indicating a beneficial effect of the encapsulation. Because of the successful encapsulation of a large number of chromophores in the silica nanoparticles (up to nearly 1×10^4 chromophores per particle), the doped silica nanospheres present bright fluorescence under both mono and biphotonic excitation with unprecedented OPEF and TPEF cross-sections (respectively $\epsilon\Phi \approx 2 \times 10^8$ M^{-1} cm^{-1} and $\sigma_2\Phi \approx$ 10 MGM). Such water-soluble fluorescent nanoparticules are particularly promising for applications relying on sensitive detection via fluorescence (in particular by two-photon excitation). Along this line, we are currently investigating surface modification of these nanoparticles for the targeting of cancer cells with the aim to create new nanotools for early diagnostic.

Experimental Section

General Information. DMF and MeCN were stored under a 4 Å molecular sieve before use. Et_3N was distilled over CaH_2. MeI and triorthotolylphosphine (TOP) were purchased from Aldrich. $Pd(OAc)_2$ and 4-vinylpyridine were purchased from Acros and both tetraethoxysilane (TEOS) and cethyltrimethylammonium bromide (CTAB) were purchased from Fluka. All products were used as received.

Synthesis of 2,7-Bis[2-(4-pyridyl) ethenyl] Fluorene 1. Product **1** was synthesized as described in the literature[44] using the following modifications.

In a sealed tube, 2,7-dibromofluorene (3.0 g, 9.26 mmol), 4-vinylpyridine (1.96 mL, 18.67 mmol), $Pd(OAc)_2$ (165 mg, 0.73 mmol), TOP (780 mg, 2.56 mmol), Et_3N (6 mL), DMF (4 mL), and MeCN (4 mL) were heated to 110 °C for 30 h. The reaction was then diluted with water and the aqueous phase was washed with CH_2Cl_2 and extracted with $CHCl_3$. The $CHCl_3$ phase was dried over $MgSO_4$, filtered over a pad of celite, and evaporated to afford an orange powder (2.9 g, 7.87 mmol, 85%).

Synthesis of 2,7-Bis[2-((4-N-methyl)pyridin-1-iumyl) ethenyl] Fluorene iodide 2. MeI (5 mL, 80.8 mmol) was added to a suspension of **1** (3.0 g, 8.1 mmol) in 50 mL of CH_3CN. The mixture was refluxed for 12 h and then cooled. The resulting precipitate was filtered and washed with CH_3CN to give a red solid (3.2 g, 4.9 mmol, 60%).

Melting point: 325 °C.

^{1}H NMR (DMSO d6), 200 MHz: 8.89 (d, ^3J = 6.7 Hz, 4H); 8.26 (d, ^3J = 6.6 Hz, 4H); 8.12 (d, ^3J = 7.9 Hz, 2H); 8.06 (s, 2H); 8.05 (d, ^3J = 20 Hz, 2H); 7.81 (d, ^3J = 9.4 Hz, 2H); 7.64 (d, ^3J = 16.4 Hz, 2H); 4.29 (s, 6H), 4.00 (s, 2H).

^{13}C NMR (DMSO d6), 50 MHz: 153.4; 146.0; 145.6; 143.5; 141.7; 135.4; 128.7; 125.5; 124.3; 123.9; 122.2; 47.8; 37.2.

High-resolution mass spectroscopy (FAB+, NBA matrix): m/z = 402.2088 (calcd 402.2096).

FT-IR (KBr), ν cm^{-1}: 3023; 1642; 1618; 1601; 1558; 1515; 1468; 1423; 1342; 1209; 1186; 1129; 1049; 978; 827.

UV (ethanol): λ_{max} = 425 nm ($\epsilon = 6.2 \times 10^4$ M^{-1} cm^{-1}).

UV (H_2O): λ_{max} = 414 nm ($\epsilon = 5.9 \times 10^4$ M^{-1} cm^{-1}).

Synthesis of 2,7-Bis[2-(4-pyridyl) ethenyl]-9,9-dihexyl Fluorene 4. 2,7-Diiodo-9,9-dihexylfluorene **3** (2.0 g, 3.05 mmol), $Pd(OAc)_2$ (30.6 mg, 0.136 mmol), and TOP (207.6 mg, 0.682 mmol) were dissolved in DMF (2.5 mL) and AcOEt (2.5 mL). 4-Vinylpyridine (0.72 mL, 6.82 mmol) and Et_3N (1.19 mL, 8.53 mmol) were added. The mixture was heated to 100 °C for 48 h under stirring. The mixture was diluted with water and extracted with CH_2Cl_2. The organic extracts were washed with brine, dried over $MgSO_4$, filtered, and evaporated. The residue was purified by flash chromatography over silica (eluent, 98:2 $CHCl_3$:MeOH) to afford **4** (759 mg, 1.40 mmol, 46%).

^{1}H NMR ($CDCl_3$), 200 MHz: 8.63 (d, $J = 6.0$ Hz, 4H); 7.76 (d, $J = 7.9$ Hz, 4H); 7.6–7.2 (m, 10H); 7.58 (d, $J = 11.7$ Hz, 4H); 7.13 (d, $J = 16.2$ Hz, 4H); 2.2–1.9 (m, 4H); 1.3–0.5 (m, 22H).

^{13}C NMR ($CDCl_3$), 50 MHz: 152.2; 150.4; 145.4; 141.9; 135.8; 134.3; 126.8; 125.7; 121.5; 120.7; 120.4; 55.6; 40.8; 31.9; 30.1; 24.2; 23.0; 14.4.

High-resolution mass spectroscopy (FAB+, NBA matrix): 541.3591 (calcd 541.3583).

FT-IR (KBr), ν cm^{-1}: 2923; 2853; 1626; 1591.

Elemental anal.: C, 85.57 (calcd 86.60%); H, 7.61 (calcd 8.22%); N, 4,92 (calcd 5.18).

Synthesis of 2,7-Bis[2-((4-N-methyl)pyridin-1-iumyl) ethenyl]-9,9-dihexyl Fluorene Iodide *5*. Compound **4** (0.5 g, 0.93 mmol) was heated overnight at 40 °C with MeI (1.3 mL, 2.05 mmol) in MeCN (15 mL). Volatiles were evaporated, and the resulting red solid was dried under a vacuum (728 mg, 0.88 mmol, 95%).

^{1}H NMR (DMSO d6), 200 MHz: 8.88 (d, $J = 6.0$ Hz, 4H); 8.24 (d, $J = 6.0$ Hz, 4H); 8.13 (d, $J = 16.0$ Hz, 2H); 8.02 (d, $J = 8.00$ Hz, 2H); 7.92 (s, 2H); 7.79 (d, $J = 8.00$ Hz, 2H); 7.65 (d, $J = 16.0$ Hz, 2H); 4.28 (s, 6H); 2.2–1.9 (m, 4H); 1.3–0.4 (m, 22H).

^{13}C NMR (DMSO d6), 50 MHz: 153.4; 152.5; 145.9; 143.0; 141.9; 135.8; 129.0; 124.3; 123.9; 123.2; 122.0; 55.7; 47.8; 31.7; 29.7; 24.3; 22.8; 14.6.

High-resolution mass spectroscopy (FAB+, NBA matrix): m/z = 570.3995 (calc. 570.3974).

FT-IR (KBr), ν cm^{-1}: 3100; 2922; 2851; 1617; 1598; 1515; 1465; 1340; 1184; 829.

UV (ethanol): $\lambda_{max} = 423$ nm.

UV (H_2O): $\lambda_{max} = 418$ nm.

Synthesis of Dye-Doped Silica Nanoparticles NP-2 and NP-5. CTAB (686 mg, 1.9 mmol) was dissolved in 40 mL of a 0.2 M aqueous solution of NaOH at the controlled temperature of 25 °C. Chromophore **2** or **5** (4 mg) was then dissolved in this solution, which turned yellow. TEOS (3.5 mL, 15.7 mmol) was added dropwise under stirring. After 40 s, water (250 mL) was added to the mixture, which was left stirring for 6−8 min. Neutralization (pH 7) was then achieved by addition of a 0.2 M aqueous HCl solution. The nanoparticles were separated from the solvent by centrifugation (three times, washed with EtOH) and purified by Soxhlet extraction with ethanol for 24 h. After drying under a vacuum, the average weight of a batch of nanoparticles was around 750 mg.

BET. Specific surface areas were determined by Brunauer–Emmett–Teller (BET)[70] method on a Micromeritics ASAP 2010 analyzer (using 74 points and strating from 0.01 as value for the relative pressure) and the average pore diameters were calculated by the BJH method.

TEM. TEM measurements were carried out with a JEOL 1200 EXII microscope at 100 kV.

UV/Vis Spectroscopy and Monophotonic Fluorimetry. All measurements were carried out at 298 K, using a standard 1 cm path length quartz cuvettes. Final data treatment (e.g., automated baseline subtraction, Figure 5) and visualization was done using the IGOR Pro 5 software package (Wavemetrics, Lake Oswego OR, USA). The UV/vis absorption photometer is a Jasco V-570 instrument. Steady-state fluorescence emission and anisotropy measurements were made using an Edinburgh FLS920 fluorimeter (450W Xe lamp, Hamamatsu R928P photon counting detector, simple monochromators). The usual detection sensitivity corrections were applied to the fluorescence spectra, and all emission spectra are expressed as relative photon flux per unit wavelength versus wavelength. Quantum yields were measured on dilute solutions (absorbance <0.1) using quinine bisulfate in aqueous H_2SO_4 as a reference, according to a standardized procedure.[71] Time-resolved fluorescence measurements were done on the same instrument in time-correlated single photon counting mode using an Edinburgh Instruments EPL-440 pulsed diode laser as the excitation source ($\lambda_{exc} = 443.5$ nm). Detection of the emitted light was at 530 nm through a polarizer at magic angle (54.7°). The overall instrument response was 1 ns fwhm. The measured decay curves were analyzed using iterative reconvolution of mono- and biexponential decay curves with the instrument response (recorded at the excitation wavelength using a Ludox scatterer).

Two-Photon Excited Fluorescence Spectroscopy. Two-photon excited fluorescence spectroscopy was performed using a mode-locked Ti:sapphire laser generating 150 fs wide pulses at a 76 MHz rate, with a time-averaged power of several hundreds of mW (Coherent Mira 900 pumped by a 5 W Verdi). The laser light is attenuated using a combination of half-wave plates and a Glan-laser polarizer and the excitation power is further controlled using neutral density filters of varying optical density mounted in a computer-controlled filter wheel. After 5-fold expansion through two achromatic doublets, the laser beam is focused by a microscope objective (10x, NA 0.25, Olympus, Japan) into a standard 1 cm absorption cuvette containing the sample. The applied average laser power arriving at the sample was between 0.5 and 15 mW, leading to a time-averaged light flux in the focal volume on the order of 0.1–1 mW/μm^2. The generated fluorescence is collected in epi-fluorescence mode, through the microscope objective, and reflected by a dichroic mirror (675dcxru, Chroma Technology Corporation, USA). Residual excitation light is removed using a barrier filter (e650–2p, Chroma) and the fluorescence is coupled into a 600 μm multimode fiber by an achromatic doublet. The fiber is connected to a compact CCD-based spectrometer (BTC112-E, B&WTek, USA), which measures the two-photon excited emission spectrum. The emission spectra are corrected for the wavelength-dependence of the detection efficiency using correction factors established through the measurement of reference compounds having known fluorescence emission spectra. Briefly, the setup allows for the recording of corrected fluorescence emission spectra under multiphoton excitation at variable excitation power and wavelength.

Absolute values for the two-photon excitation action cross-sections $\sigma_2\Phi$ were obtained according to the method described by Xu & Webb, using 1×10^{-4} M fluorescein in 0.01 M NaOH(aq) as a reference,[68] applying corrections for the refractive index of the solvent.[72] In the 700–720 nm excitation range, refined reference values for fluorescein were used.[67]

Dynamic Light Scattering. Dynamic light scattering (DLS) experiments were run using a Malvern spectrogoniometer, Autosizer 4800, with a 50 mW laser source operating at 532 nm.

The time dependence of the intensity fluctuation is measured and analyzed using a 7132 digital correlator, which allows us to determine the intensity autocorrelation function. The exponential decay of the correlation function is characteristic of the diffusion coefficient of the particles.

The general formula for the intensity autocorrelation function is expressed as

$$g^{(2)}(t) = 1 + \beta\left|g^{(1)}(t)^2\right|$$

where $g^{(2)}(t)$ is the normalized second-order correlation function, β is a constant parameter, $g^{(1)}(t)$ is the normalized first-order

(70) Brunauer, S.; Emmet, P. H.; Teller, E. *J. Am. Chem. Soc.* **1938**, *60*, 309–319.

(71) Eaton, D. F. *Pure Appl. Chem.* **1988**, *60*, 1107–14.

(72) Werts, M. H. V.; Nerambourg, N.; Pelegry, D.; Le Grand, Y.; Blanchard-Desce, M. *Photochem. Photobiol. Sci.* **2005**, *4*, 531–538.

correlation function, and t is the delay time. The measured normalized time correlation function $g^{(1)}(t)$ was analyzed by use of the method of cumulants, where unimodal distribution of relaxation time is considered. The method of cumulants gives the diffusion coefficient of the particles, D.

$$\ln g^{(1)}(t) = 1 - \Gamma_1 t + \Gamma_2 t^2/2 - \cdots$$

Γ_1 is the first cumulant, which is related to the translational diffusion coefficient via $\Gamma_1 = Dq^2$, where q is the scattering vector. $q = (4\pi n_0/\lambda)\sin(\theta/2)$, where λ is the incident laser wavelength, n_0 is the refractive index of the sample, and θ is the angle at which the detector is located with respect to the sample cell. The polydispersity index (PDI) is the Γ_2/Γ_1^2 ratio. The values of the hydrodynamic diameters were calculated from the decay times using the Stokes–Einstein equation: $D_h = k_B T/3\pi\eta D$, where k_B is the Boltzmann constant, T is absolute temperature, and η is the solvent viscosity.

All samples were filtered through Teflon filters of 0.8 μm pore size.

The scattering measurements were done at 90°. The DLS measurements were all performed at a constant temperature of 25 °C. The experimental duration for each experiment was 3−15 min depending upon the scattering intensity.

Acknowledgment. This project was sponsored by ACI nanobioscience NR 077. V.L. thanks CNRS and Region Languedoc Roussillon for a doctoral fellowship.The Rennes group acknowledges equipment grants from CNRS, Rennes Métropole, and Université de Rennes 1, as well as a doctoral fellowship to N.N. from the French Ministry of Higher Education and Research.

CM703487B